Modeling and Control of a Four-port DC-DC Converter for a Hybrid Energy System

Jianwu Zeng[1*], Jiahong Ning[1], Taesic Kim[2], and Vincent Winstead[1]
1. Department of Electrical and Computer Engineering and Technology, Minnesota State University, Mankato, MN, USA
2. Department of Electrical Engineering and Computer Science, Texas A&M University-Kingsville, TX, USA
jianwu.zeng@mnsu.edu; jiahong.ning@mnsu.edu; taesic.kim@tamuk.edu; vincent.winstead@mnsu.edu

***Abstract*—This paper presents modeling and controllers design of a four-port DC-DC converter for integration of a hybrid energy system which includes a photovoltaic (PV) panel, wind turbine generator (WTG), and a battery. A small signal model is first derived from the differential equations of the converter in different operation stages. Based on this model, four controllers are developed to control the voltage and current of the battery, and the output voltage of the converter while eliminating the coupling item between two voltage loops. Simulation and experimental studies are carried out and validate that these controllers are capable of controlling the power flow of renewable energy sources, battery, and the load. Besides, they can protect the battery from over-charging and over-discharging while maintaining constant DC link voltage.**

***Keywords*—Battery, DC-DC converter, four-port, hybrid energy system, photovoltaic (PV), renewable energy.**

I. INTRODUCTION

Renewable energy such as wind and solar energy has been attracted much attention due to its clean and alternative characteristics [1]. Since a hybrid wind and solar energy system has a better generation profile than standalone wind or solar system [2], a hybrid energy system is more preferable than that using the single energy source. However, due to the intermittent characteristics of renewable energy sources (RES), an energy storage device, such as a battery, is commonly used together with the RES. In such a multiple hybrid energy system, power converters with at least one bidirectional port play an important role in managing the power flow of energy sources as well as their integration to the electric grid [3],[4].

There are two ways to integrate these distributed energy sources. The traditional way is to use an individual converter for each source, i.e., one converter for each energy source; the other is to use an integrated multiple ports converter which shares some components. Although the control methods in the first solution is quite simple, the latter solution is preferable due to its relatively lower cost and higher efficiency than the traditional solution [5]-[7].

A variety of multiport bidirectional DC-DC converters were proposed for grid integration of RES [8]-[11]. These topologies either use too many active switches or degrade the battery lifetime due to the use of high-frequency charge/discharge profiles for the battery. For example, in [12], the battery was both charged and discharged within a switching period. Such a high-frequency charge/discharge has a negative effect on the battery lifetime. Furthermore, compared to the effort spent on the three-port converters, less work has been done on renewable integration with four-port converters. The four-port converter is usually derived by extending the existing three-port converter with extra branch thus extra power electronics device is required [12]. In this paper, the four-port converter is derived from a three-port converter by separating an existing phase-shift topology into two independent half-bridge converters [13]. Therefore, compared to the three-port phase-shift converter, no extra power electronics devices are required in the proposed four-port converter.

However, the control strategy of the four-port converter is more complex than that using multiple individual converters because it is a multi-input multi-output (MIMO) system and usually contains coupling variables between control loops [14]. This coupling system requires properly designed controllers to eliminate its coupling items so that each controller can regulate the power flow of its corresponding source independently, which is usually realized by decoupling controllers or networks. To design theses controllers, the model of the four-port converter should be derived first.

This paper presents modeling and controllers design of the proposed four-port DC-DC converter for a hybrid wind, solar, and battery system. The small-signal model is first derived from the differential equations. Based on the model, four controllers are designed to regulate the power flow of the two renewable energy sources, i.e., photovoltaic (PV) panel and wind turbine generator (WTG), battery, and the output voltage of the converter. Simulation and experimental results are provided to validate the proposed controllers when the converter works in the different modes of the battery, e.g., constant current mode and constant voltage mode. Besides, the DC link voltage is maintained to be a constant value.

Project funding provided by customers of Xcel Energy through a grant from the Renewable Development Fund.

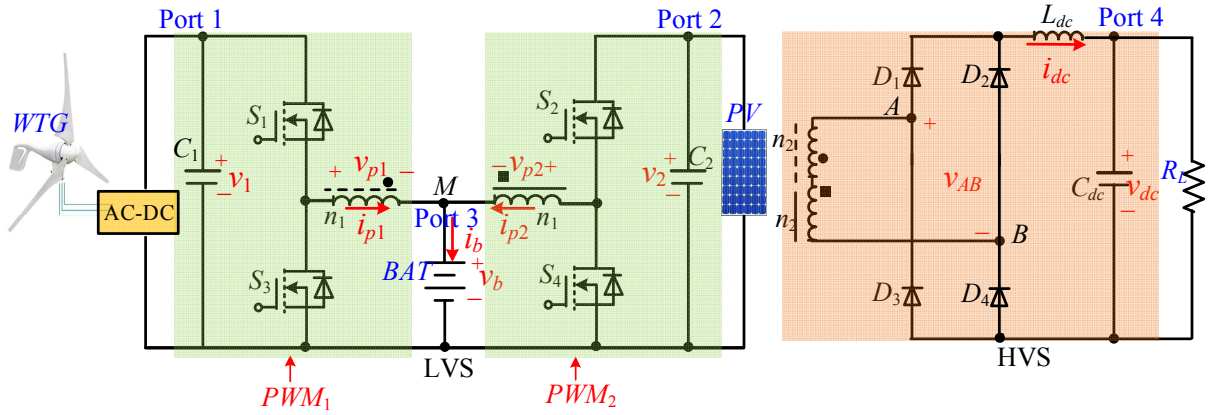

Fig. 1. Topology of the proposed four-port DC-DC converter.

II. Modeling of The Four-port Converter

Fig. 1 shows the topology of the proposed four-port DC-DC converter which is integrated with a WTG, PV panel, battery, and a inverter which is simply represented by a resistive load. The converter consists of two half bridges where each bridge is controlled by two independent PWMs, i.e., PWM1 and PWM2.

According to the state of the switches, the converter has four different operation stages and its waveforms are shown in Fig. 2. More details of differential equations in these four stages can be found in [13]. With the derived differential equations at the different stages, the state-space average model within a switching period can be expressed as follows:

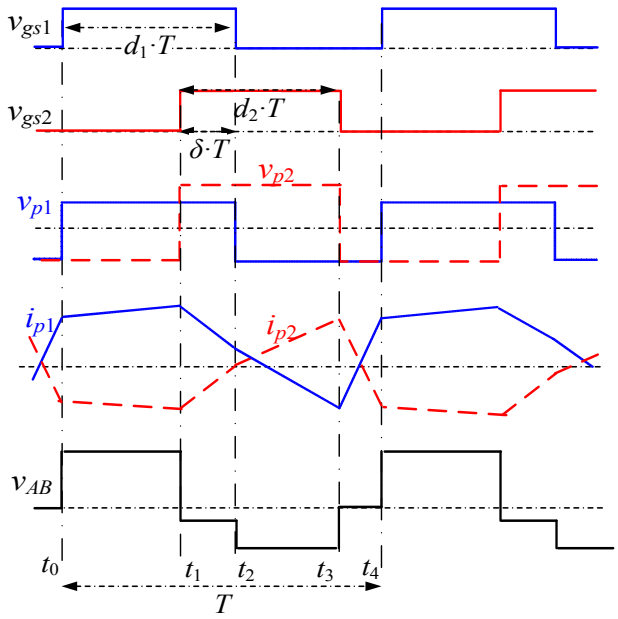

Fig. 2. Steady state waveform of the converter.

$$\begin{cases} \dfrac{di_b}{dt} = \dfrac{V_1 \cdot d_1 + V_2 \cdot d_2 - 2 \cdot v_b}{L_m} \\ \dfrac{dv_b}{dt} = \dfrac{i_b - (v_b - V_{boc})/r_b}{C_b} \\ \dfrac{di_{dc}}{dt} = \dfrac{n \cdot [V_1 \cdot d_1 + V_2 \cdot d_2 - 2V_{12m} \cdot \delta] - i_{dc} \cdot r_{dc} - v_{dc}}{L_{dc}} \\ \dfrac{dv_{dc}}{dt} = \dfrac{i_{dc}}{C_{dc}} - \dfrac{v_{dc}}{RC_{dc}} \end{cases} \quad (1)$$

where L_m is the inductance on the primary side of the transformer; V_1 and V_2 are steady state values of v_1 and v_2, respectively; V_{boc} is the open circuit voltage of the battery; r_b and r_{dc} are resistance of battery and L_{dc}, respectively; δ is the phase shift angle as defined in Fig. 2 and $\delta \in [0, d_1]$; n (= n_2/n_1) is the turns ratio of the secondary and primary side of the transformer; $V_{12m} = \min\{V_1, V_2\}$.

According to the voltage second balance of two transformers, $V_1 \cdot d_1 = V_2 \cdot d_2 = V_b$, where V_b is the average battery voltage. By introducing $d_1 = D_1 + d$ and $d_2 = D_2 + (V_1/V_2)\, d$, the small-signal model with $\dot{x} = A \cdot x + B \cdot u$ form can be found as follows:

$$\dot{x} = \underbrace{\begin{bmatrix} 0 & \frac{-2}{L_m} & 0 & 0 \\ \frac{1}{C_b} & \frac{-1}{r_b C_b} & 0 & 0 \\ 0 & 0 & \frac{-r_{dc}}{L_{dc}} & \frac{-1}{L_{dc}} \\ 0 & 0 & \frac{1}{C_{dc}} & \frac{-1}{R \cdot C_{dc}} \end{bmatrix}}_{A} \cdot x + \underbrace{\begin{bmatrix} \frac{2V_1}{L_m} & 0 \\ 0 & 0 \\ \frac{2nV_1}{L_{dc}} & \frac{-2nV_{12m}}{L_{dc}} \\ 0 & 0 \end{bmatrix}}_{B} \cdot \begin{bmatrix} d \\ \delta \end{bmatrix} \quad (2)$$

where $x = [i_b, v_b, i_{dc}, v_{dc}]^T$ and $u = [d, \delta]^T$. Based on the derived model, the transfer functions of battery and output voltage can be further derived as follows:

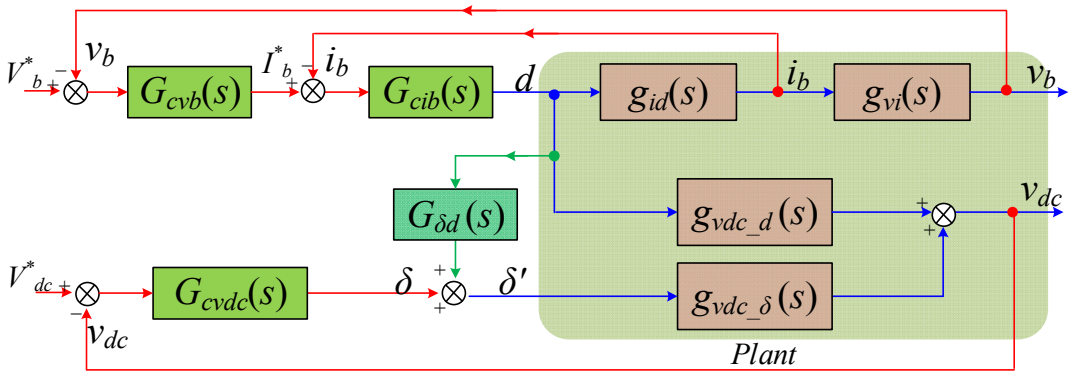

Fig. 3. Signal flows of the controllers and plant.

$$g_{id} = \frac{i_b(s)}{d(s)} = \frac{\frac{2V_1}{L_m}\left(s + \frac{1}{r_b C_b}\right)}{s^2 + \frac{1}{r_b C_b}\cdot s + \frac{2}{L_m C_b}} \tag{3}$$

$$g_{vi}(s) = \frac{v_b(s)}{i_b(s)} = \frac{r_b}{r_b \cdot C_b \cdot s + 1} \tag{4}$$

$$g_{vdc\_d}(s) = \frac{v_{dc}(s)}{d(s)} = \frac{2n \cdot V_1}{L_{dc} \cdot C_{dc}} \cdot \frac{1}{\Delta} \tag{5}$$

$$g_{vdc\_\delta}(s) = \frac{v_{dc}(s)}{\delta(s)} = \frac{2n \cdot V_{12\,m}}{L_{dc} \cdot C_{dc}} \cdot \frac{1}{\Delta} \tag{6}$$

where

$$\Delta = s^2 + \left(\frac{1}{RC_{dc}} + \frac{r_{dc}}{L_{dc}}\right)\cdot s + \frac{1 + r_{dc}/R}{L_{dc}C_{dc}} \tag{7}$$

As indicated in (5) and (6), the DC link voltage v_{dc} is not only related with d, but δ as well. Since the duty cycle of d affects the battery current and voltage, it is necessary to develop a decoupling controller so that d and δ can be used for controlling the battery current and DC link voltage, respectively.

III. Controllers Design

Fig. 3 shows the signal flows of the overall system with four controllers: $G_{cvb}(s)$ and $G_{cib}(s)$ are used for controlling v_b and i_b, respectively; $G_{cvdc}(s)$ is to control v_{dc} while $G_{\delta d}(s)$ is used for eliminating the influence of d toward to v_{dc} through $g_{vdc\_d}(s)$. As shown in Fig. 3, the plant is a multivariable system with the coupling term $g_{vdc\_d}(s)$, which indicates the DC link voltage is not only related with d, but δ as well. To eliminate the influence of d toward v_{dc}, the decoupling controller $G_{\delta d}(s)$ can be calculated from g_{vdc_d} and g_{vdc_δ} as follows:

$$G_{\delta d}(s) = -\frac{g_{vdc\_d}(s)}{g_{vdc\_\delta}(s)} = -\frac{V_1}{V_{12\,m}} \tag{8}$$

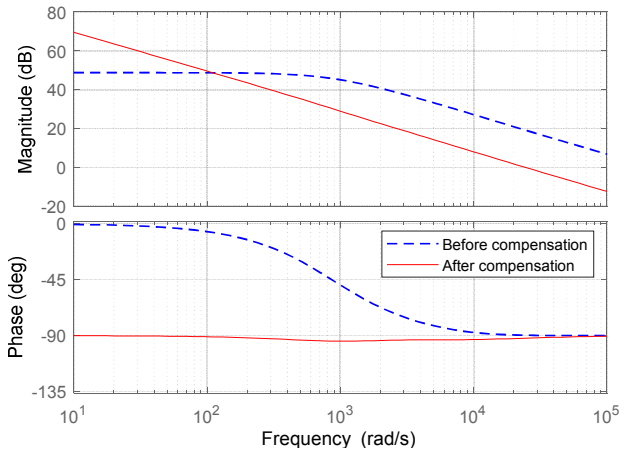

(a)

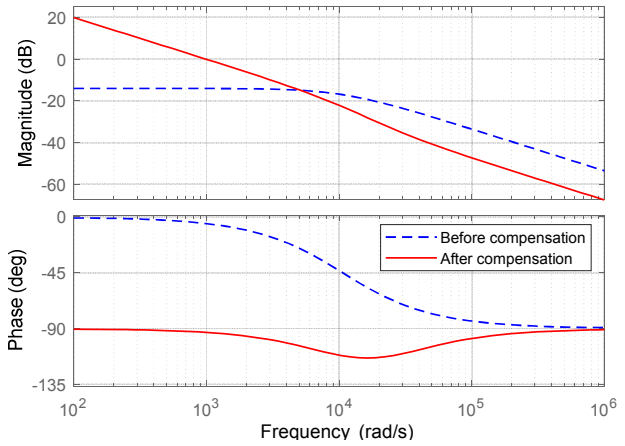

(b)

Fig. 4. Bode plots of battery loop before and after compensation. (a) battery current loop; (b) battery voltage loop.

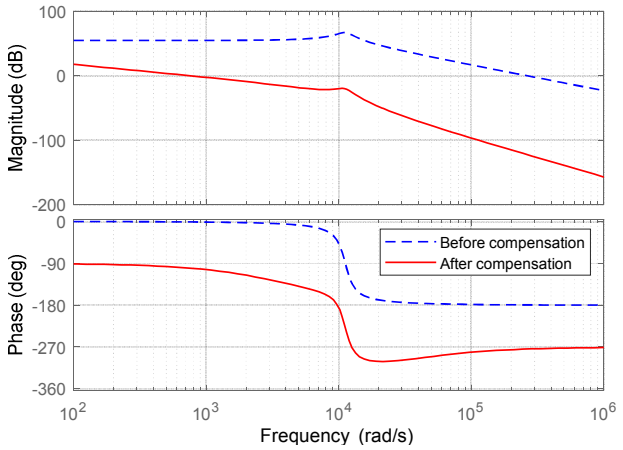

Fig. 5. Bode plots of DC link voltage loop with and without $G_{cvdc}(s)$.

With the decoupling controller, the controllers of battery and DC link voltage then can be designed independently. $G_{cib}(s)$ and $G_{cvb}(s)$ then can be easily designed with the transfer functions of $g_{id}(s)$ and $g_{vi}(s)$. Fig. 6 shows the bode plot with and without using controllers $G_{cib}(s)$ and $G_{cvb}(s)$. As shown in Fig. 6 (a), 20 kHz cutoff frequency of the original battery current loop is too high and need to be decreased. Then $G_{cib}(s)$ is derived by designing the cutoff frequency around 3 kHz while maintaining phase margin more than 40 degrees. Similarly, the $G_{cvb}(s)$ is determined by placing its cutoff frequency less than 1/10 of its current loop, i.e., 150 Hz in this paper. Then the following controllers can be found:

$$G_{cib}(s) = \frac{0.06 \cdot (s + 1000)}{s} \tag{9}$$

$$G_{cvb}(s) = \frac{0.014 \cdot (s + 7 \times 10^4)}{s} \tag{10}$$

The DC link voltage is designed based on $g_{vdc\_\delta}(s)$. Fig. 5 shows the bode plot with and without $G_{cvdc}(s)$. The original

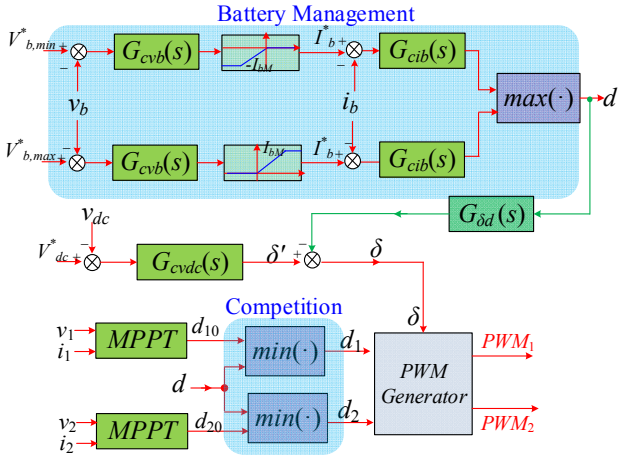

Fig. 6. Competitive organization of controllers.

voltage loop is a secondary system and has a resonant component, its cutoff frequency is around 47 kHz which needs to be decreased. To decrease the cutoff frequency as well as suppress the gain at its resonant frequency, i.e., 1.6 kHz, a PI controller with a low pass filter is selected. As shown in Fig. 5, $G_{cvdc}(s)$ is determined by suppressing the gain at 1.6 kHz less than -20 dB as well as placing the cutoff frequency around 150 Hz.

$$G_{cvdc}(s) = \frac{0.3 \cdot (s + 2.7 \times 10^4)}{s \cdot (s + 3900)} \tag{11}$$

Once these four controllers are designed, it is necessary to organize them in a correct way to meet certain requirements, for example, the maximum power point tracking (MPPT) for renewable energy sources, over voltage or current protection for the battery. Fig. 6 shows the diagram of controllers' organization. As shown in Fig. 6, the battery management system prevents the battery from over voltage and overcurrent conditions during operation. For example, when the battery works in the charge mode, the predefined maximum allowance voltage and current, i.e., $V^*_{b,max}$ and I_{bM} avoid the over voltage and over current charge. Similarly, the minimum battery voltage $V^*_{b,min}$ and battery current $-I_{bM}$ prevents it from over discharge. Since the renewable energy sources connected to Port 1 and Port 2 are required to work properly with the battery, e.g., work in MPPT mode or limit the power if more power is generated, the four controllers are organized with two MPPT controllers in a competitive manner. Then PWMs are generated based on d_1, d_2, and δ. It should be noted that the MPPT controllers design are beyond the scope of this paper because they are independent from the model.

IV. Simulation and Experimental Results

The simulation studies are carried out in Matlab/Simulink to testify the effectiveness of these controllers. In the simulation, the open-circuit voltage (V_{oc}) and the short-circuit current (I_{sc}) of the PV panel are 75 V and 10 A (at 25℃, 1 kW/m^2) respectively, V_{mpp} = 60 V, the nominal voltage of WTG simulator and battery are 48 V and 24 V, respectively, and the switching frequency is 100 kHz. To demonstrate the effectiveness of the controllers of the battery loops, the maximum battery charge voltage ($V^*_{b,max}$) and current (I_{bM}) are set to be 26.6 V and 25 A, respectively. The desired DC-link voltage ($V_{dc}{}^*$) is 180V.

Fig. 7 shows the simulation results when the wind speed and solar radiation changes. As shown in Fig. 7, the battery voltage is below 26.6 V which is the maximum charge voltage. The output of the $G_{cvb}(s)$ is positive and is limited to be I_{bM} (= 25 A), the battery works in the constant current mode. This mode lasts until t = 0.42 sec when v_b = 26.6 V. After that, the output of the $G_{cvb}(s)$ decreases from I_{bM} and the charge voltage is clamped to 26.6 V, the battery works in the constant voltage mode.

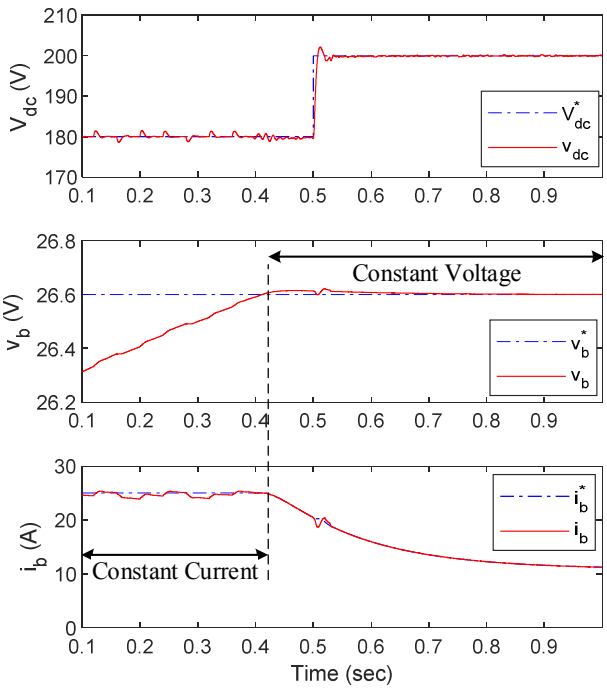

Fig. 7. Simulation results with all controllers.

To test the DC-link voltage controller, the reference of v_{dc} is changed from 180 V to 200 V at t = 0.5 sec, as shown in Fig. 7, v_{dc} quickly reaches to its new reference value of 200 V, which validates the effectiveness of $G_{cvdc}(s)$.

During the whole simulation period, v_{dc} does not change with the battery voltage or current unless its reference voltage is changed. In other words, the response of the battery loop does not affect the DC link voltage, which testified the effectiveness of the decoupling controller $G_{\delta d}(s)$.

A 1 kW prototype was built to validate the proposed four-port DC-DC converter. Fig. 8 shows the overall experimental setup. The four-port DC-DC converter is connected to a BK PVS60085MR PV simulator; a DC voltage source is used to simulate the WTG. All real-time control algorithms are implemented in an eZdsp F28335 control board.

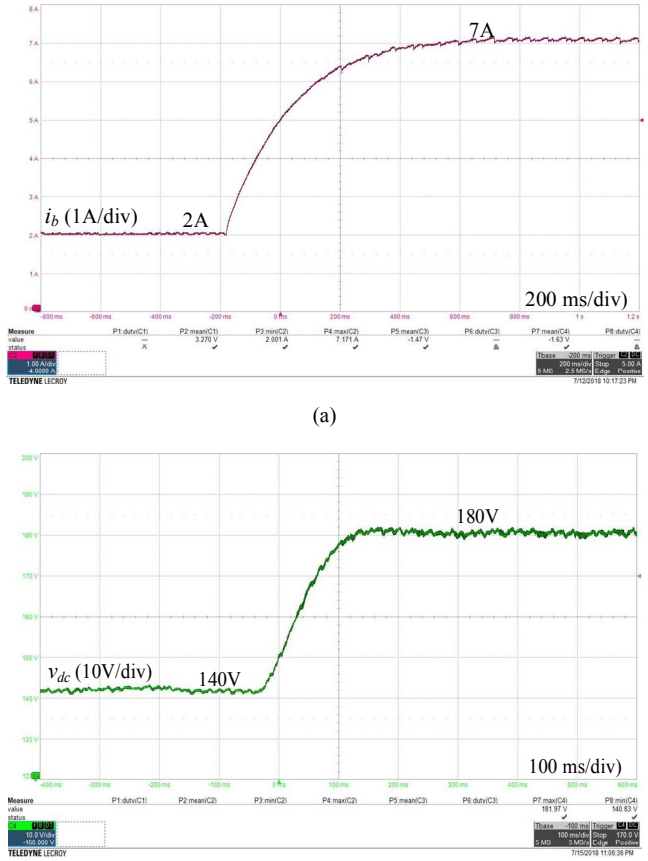

Fig. 9. Measured battery current (i_b) and DC-link voltage (v_{dc}) response with controllers. (a) i_b; (b) v_{dc}.

Fig. 9 shows the measured responses of the battery current

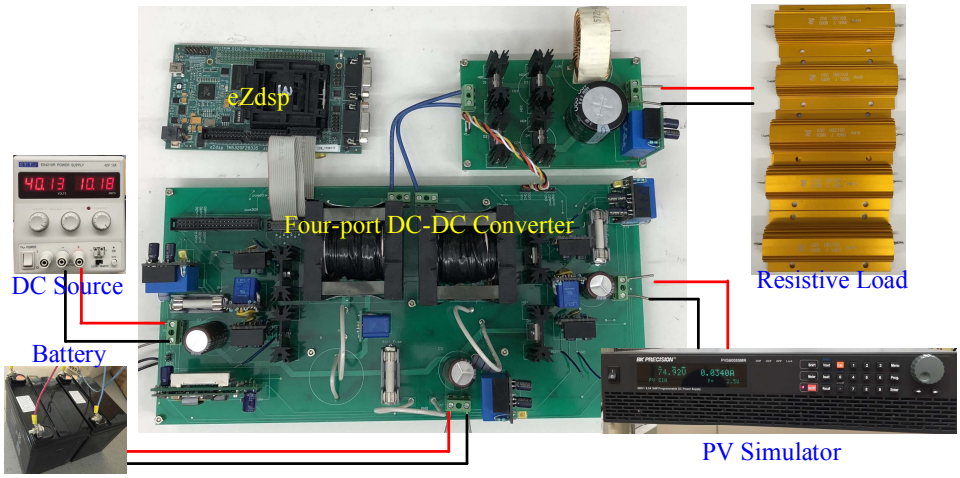

Fig. 8. Experimental setup.

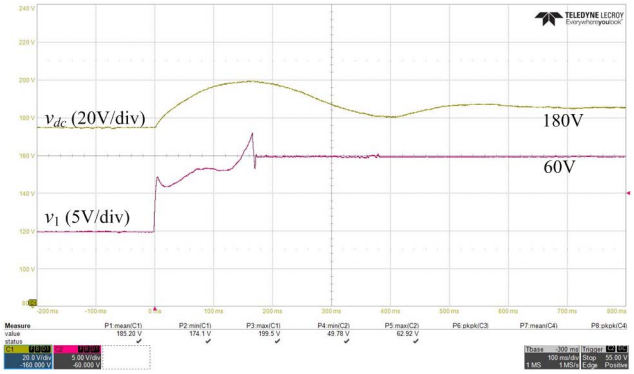

Fig. 10. Measured DC link voltage (v_{dc}) when v_1 is step changed.

(i_b) and DC-link voltage (v_{dc}). At $t = -200\ ms$, the reference current is changed from 2 A to 7A, as shown in Fig. 9 (a), the transient state of i_b lasts approximately 0.6 s, during which i_b increases from 2 A to new reference value 7 A, which indicates the effectiveness of $G_{cib}(s)$. Similarly, the measured v_{dc} is changed from 140 V to 180 V within 100 *ms* as shown in Fig. 9 (b), which demonstrates the function of $G_{cvdc}(s)$ implemented with phase-shift technique.

Fig. 10 shows the measured waveform of v_{dc} when the voltage of port 1 is suddenly changed from 45 V to 60 V. v_{dc} has 20-V overshoot during the transient, after 500 ms, it drops back to 180 V, which again validates the effectiveness of $G_{cvdc}(s)$.

V. CONCLUSIONS

This paper presents a small-signal model and controllers design of a four-port DC-DC converter for hybrid wind, solar, and battery system. Based on the model, controllers were designed to control the voltage and current of battery, the DC link voltage, and eliminate the coupling item between the battery and DC link voltage. Simulation and experimental results further show that the designed controllers are not only capable of controlling the battery and work in the different modes depending on its SOC, i.e., constant current mode and constant voltage mode, but also regulating the DC link voltage to a constant value.

REFERENCES

[1] S. Bull, "Renewable energy today and tomorrow," *Proc. IEEE*, vol. 89, no. 8, pp. 1216-1226, Aug 2001.

[2] S. Venkataraman, C. Ziesler, P. Johnson, and S. Van Kempen, "Integrated wind, solar, and energy storage: Designing plants with a better generation profile and lower overall cost," *IEEE Power and Energy Magazine*, vol. 16, no. 3, pp. 74-83, May-June 2018.

[3] H. Wu, R. Chen, J. Zhang, Y. Xing, H. Hu, and H. Ge, "A family of three-port half-bridge converters for a stand-alone renewable power system," *IEEE Trans. Power Electron.*, vol. 26, no. 9, pp. 2697-2706, Sept. 2011.

[4] E. Muljadi, "Power electronics: Roles in renewable energy generation-challenges and opportunities," in *Proc. Power and Energy Society General Meeting*, Boston, MA, July 2016.

[5] V. N. S. R. Jakka, A. Shukla, and G. D. Demetriades, "Dual-transformer-based asymmetrical triple-port active bridge (DT-ATAB) Isolated DC-DC converter," *IEEE Trans. Ind. Electron.*, vol. 64, no. 6, pp. 4549-4560, June 2017.

[6] J. Zeng, W. Qiao and L. Qu, "An isolated three-port bidirectional DC-DC converter for photovoltaic systems with energy storage," *IEEE Trans. Ind. Appl.*, vol. 51, no. 4, pp. 3493-3503, July-Aug. 2015.

[7] H. Tao, A. Kotsopoulos, J. Duarte, and M. Hendrix, "Family of multiport bidirectional DC-DC converters," in *IEE Proc. Electric Power Appl.*, vol. 153, no. 3, pp. 451-458, May 2006.

[8] H. Wu, K. Sun, R. Chen, H. Hu, and Y. Xing, "Full-bridge three-port converters with wide input voltage range for renewable power systems," *IEEE Trans. Power Electron.*, vol. 27, no. 9, pp. 3965-3974, Sept. 2012.

[9] Z. Ding, C. Yang, Z. Zhang, C. Wang, and S. Xie, "A novel soft-switching multiport bidirectional DC-DC converter for hybrid energy storage system," *IEEE Trans. Power Electron.*, vol. 29, no. 4, pp. 1595-1609, April 2014.

[10] K. Itoh, M. Ishigaki, N. Yanagizawa, S. Tomura, and T. Umeno, "Analysis and design of a multi-port converter using a magnetic coupling inductor technique," in *Proc. Energy Convers. Congr. Expo.*, Sept. 2013, pp. 4713-4718.

[11] Z. Qian, O. Abdel-Rahman, J. Reese, H. Al-Atrash, and I. Batarseh, "Dynamic analysis of three-port DC/DC converter for space applications," in *Proc. IEEE Appl. Power Electron. Conf. Exposit.*, Feb. 2009, pp. 28-34.

[12] Z. Qian, O. Abdel-Rahman, and I. Batarseh, "An integrated four-port DC/DC converter for renewable energy application," *IEEE Trans. Power Electron.*, vol. 25, no. 7, pp. 1877-1887, Jul. 2010.

[13] J. Zeng, T. Kim, and V. Winstead, "A soft-switched four-port DC-DC converter for renewable energy integration," in *Proc. IEEE Energy Convers. Congr. Exposit.*, Portland, OR, Sept. 2018, pp. 5851-5856.

[14] C. Zhao, S. Round, and J. Kolar, "An isolated three-port bidirectional DC-DC converter with decoupled power flow management," *IEEE Trans. Power Electron.*, vol. 23, no. 5, pp. 2443-2453, Sept. 2008.